for previous aircraft of similar types. The data is also helpful for establishing task times.

Scheduled Maintenance Inspection Cost (SMIC) Module

This module will present and track current F-15 SMI costs related to the current requirements for scheduled maintenance. The U.S. Air Force model was used to derive many of the cost parameters associated with this maintenance cost model.

F-15 Work Unit Code (WUC) Data Base

This data base stores the current listings of WUC breakdowns and nomenclature for F-15 aircraft.

Phase/Special/Periodic Inspection Data Base

This data base, developed by MDA, contains scheduled inspections not related to turnaround/daily type maintenance.

Automated Computer System (ACS) Inspections

This system contains the current F-15 inspection requirements for inclusion to the SMOS central data base.

Future Work

SMOS adds software development to analyze fielded aircraft with FMECA and RCM modules interfacing with the modules already developed. Enhancements to software development currently in work will also be investigated in the future.

Conclusion

An integrated software package composed of a FMECA module, a RCM module, a SMID, a SMIC module, and an ICT module are in development. These modules provide an integrated consolidated process for rapid assessment of previous aircraft scheduled maintenance requirements, combat turnaround times, and the necessary analysis tools to provide future scheduled maintenance requirements and optimum elapsed time for ICTs. MDA has already developed PC-based SMID, ICT, SMIC, FMECA and RCM modules.

This system will identify and document current and emerging technologies available to reduce aircraft turnaround during both ground and carrier operations. It will identify candidate improvement areas to increase war fighting capabilities through increased aircraft availability; decrease mobility requirements by reducing the number of personnel and support equipment to sustain a deployed location; and decrease manpower requirements by eliminating, combining, and optifjmizing inspection requirements, therefore reducing operations and support cost. Candidate improvement areas include aircraft design areas (inertial navigation alignment, refuel, health monitoring, and enhanced methods to reduce fault diagnostics time, etc.), arresting gears, ground and deck vehicles, weapons storage/handling and storage, and maintenance operations.

Acknowledgments

The initial investigation to identify technologies/methodologies to reduce the burden of scheduled maintenance was funded by MDA as Independent Research and Development (IRAD). The use of software tools to study current aircraft gained the interest of WR-ALC which led to funding for a scheduled maintenance optimization system. Warner Robins AFB, Air Force Material Command has funded the development of the FMECA, RCM, and software development to integrate existing modules.

Reference

[1]Anderson, R. J., "Scheduled Maintenance Optimization System Study," WR-ALC/Industry R&M and Technology Symposium; Robins Air Force Base, GA, 1990.

Aerodynamic Properties of Crescent Wing Planforms

P. L. Ardonceau*
Ecole Nationale Supérieure de Mécanique et d'Aérotechnique, 86034 Poitiers, France

Introduction

SOME years ago, an interesting paper from Van Dam[1] focused attention upon a possible benefit of the so-called crescent planform. The argumentation is based on the observation that this kind of planform has been selected through millions of years of evolution by several species of "efficient" flying and swimming animals. Good examples are given by the swift wings (flapping flight) and the shark tail (carangiform motion), many other examples can be found in Ref. 1

It is obvious that any living system is very subtle machinery as compared to human designs. The wing itself must be considered as a fully "active" or "adaptative" system as opposed to the passive aircraft wing: its camber, planform, and dihedral react to any flight situation. Despite that complexity, it seems natural to question if the wing planform can have some interest for aircraft applications.

Van Dam has published several contributions on that subject.[1-4] Considering the induced drag properties of crescent wing planforms, a numerical investigation seems to demonstrate a spectacular reduction in comparison with the conventional unswept elliptical wing.[2] An 8% reduction of the induced drag coefficient ratio $K_i = C_{Di}/(C_{Di})_{\text{eff}}$ is claimed ($AR = 7$, $\alpha = 4.0$ deg), using a nonlinear surface panel method.

An experimental study undertaken later[4] shows a much smaller difference between the basic (unswept) elliptical wing and the crescent planform. The efficiency of the wing is described by means of the Oswald efficiency factor e

$$e = \frac{C_L^2}{(C_D - C_{D_0})\pi AR}$$

where C_{D_0} is the drag coefficient at zero lift, C_L is the lift coefficient, and AR is the aspect ratio of the wing. Some differences are observed between the basic (unswept) elliptical wing and the crescent wing, but the improvement is within 2 and 4%, with an estimated uncertainty of 3%.

The present work has been performed before the publication of the preceding results. The experimental variation of the lift-dependent drag with the mean sweep of several wing planforms is carefully investigated and no definite gain has been observed. It is pointed out that attempting to separate the "inviscid" induced drag from the total lift-dependent drag can lead to erroneous conclusions if only very small effects are expected.

Experimental Setup

Four wing planforms have been analytically defined by means of a chord length and a quarter-chord position law. The same elliptical chord length function is applied on every model, namely:

$$c(\eta) = c_r\sqrt{1 - \eta^2}$$

where η is the reduced spanwise coordinate, $y/(b/2)$. The root chord c_r is related to the aspect ratio $AR = b^2/s$ through

$$c_r = 4 \cdot b/(\pi \cdot AR)$$

Received April 22, 1992; revision received Feb. 20, 1993; accepted for publication March 15, 1993.

*Research Scientist, C.N.R.S. (URA 191). Member AIAA.

In order to enhance the magnitude of the induced drag in the total drag balance, a small aspect ratio of 5 is used in the present study.

A second function, f, defines the quarter chord position along the span:

$$f(\eta) = x_{0.25}/(b/2)$$

$$f(\eta) = f_0(1 - \sqrt{1 - 0.95\eta^2})$$

The numerical coefficient 0.95 prevents the local sweep to become infinite at the tip ($\eta = 1$), f_0 is deduced from the selected values of $f(\eta)$ at tip, i.e., the total backward curvature of the quarter-chord line, namely $f(1) = 0, 0.20, 0.45, 0.65$.

The resulting shapes are shown in Fig. 1. From the definitions of $c(\eta)$ and $f(\eta)$, a mean aerodynamic sweep angle can be defined:

$$\Lambda_{ma} = \frac{b^2}{2AR}\int_0^1 \Lambda(\eta)C(\eta)\,d\eta$$

where

$$\Lambda(\eta) = tg^{-1}\left(\frac{df}{d\eta}\right)$$

The values of f_0 and Λ_{ma} are summarized in Table 1.

It is seen that even for a pronounced crescent aspect, the active sweep angle remains moderate. The four models have no wing twist and no dihedral.

A conventional NACA 0012 wing section has been selected because of its "smooth" variation of the friction drag with the angle of attack. However, there is absolutely no proof that the friction drag in the swept parts of the wings can be compared to the two-dimensional wing section drag of the same profile, even at small angles of attack.

Although refined drag analysis by means of wake survey are commonly used in our laboratory, a more global investigation has been preferred as a first step. The models are

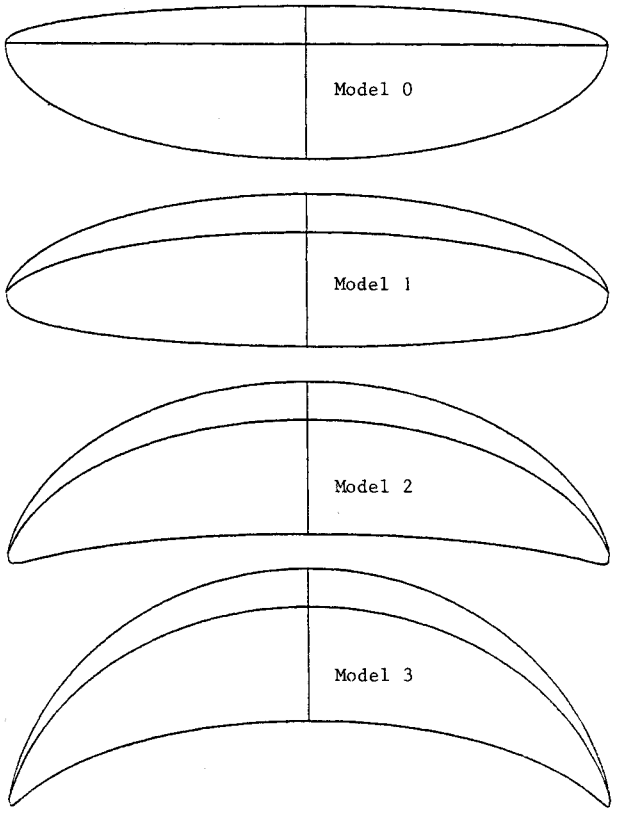

Fig. 1 Planforms geometry of the four wings under test.

Table 1 Geometric parameters of the wing planforms

Model	f_0	Λ_{ma}, deg
0	0	0
1	0.2576	8.1
2	0.5796	16.7
3	0.8372	22.3

therefore balance-mounted for measurements of the aerodynamic coefficients. The experiments are conducted in a 100-kW subsonic wind tunnel with a test section of 1.00 × 1.20 m and a large contraction ratio (20) following the low-turbulence design of the tunnel. The speed can vary from 0 to 90 m/s and is set to 60 m/s in the present study. The models are made from several bounded templets of thin plywood, hand smoothed and painted. A moderate value of the span is selected, $b = 0$, 60 m, to limit the upwash induced by the image vortices that represent the tunnel boundaries effects[5] (tunnel width = 1.0 m).

The tunnel balance is a strut-type strain-gauge balance with α and β programmed motions. The models are rigidly fixed to the balance whose axis move with the models. The aerodynamic interactions must be taken into account and each normal run is repeated with an "image" of the balance strut-mounted on the other side of the wing.[2] The Reynolds number based on the mean aerodynamic chord is 0.55×10^6, and there is no tripping of the boundary layer (natural transition). Two-hundred data points per channel are collected at each angle of attack, over a relatively long duration (5 s) to smooth out most of the tunnel instabilities.

Results and Discussion

The variation of the drag coefficient with lift coefficient is shown in Fig. 2. The data points for each model are obtained from eight nonsuccessive runs, including remounting of the models between runs. No marked difference may be seen at first sight, apart from slight decrease of the drag coefficient at zero lift with increasing sweep.

Making a refined analysis of the drag components from experimental data is not an easy task. The total drag C_D results from two contributions, the pressure drag C_{D_p} and the friction drag C_{D_f} (surface integrations over the body of the normal and tangential stresses). Direct measurements of C_{D_p} and C_{D_f} from surface integrations by means of pressure and skin friction transducers can be thought, however, a very large number of transducers is required to reach the needed accuracy. A much better accuracy could be obtained from a wake analysis: C_D is the sum of the mechanical energy (vortex drag) and of the thermal energy (total pressure losses) fed into the wake. But due to viscous transfers between mechanical and thermal forms of energy, these quantities are streamwise-dependent (the sum is invariant).

In the limit of infinite Reynolds numbers, theoretical considerations suggest that

$$\lim_{Re\to\infty}[C_D(C_L) - C_{D_0}] = \lim_{Re\to\infty}[C_{D_P}(C_L) - C_{D_{P_0}}] = kC_L^2$$

In other words, the lift-induced drag arises from the pressure drag and is a quadratic form of the lift coefficient as $Re \to \infty$. At finite Reynolds numbers the friction drag is not negligible and can contain some dependence upon C_L^2. It is moreover doubtful that the friction drag for a wing of moderate aspect ratio can be deduced from two-dimensional data of the section drag.[4]

To avoid this cumbersome situation, it is suggested to perform an analysis in terms of total drag dependence upon the lift coefficient, leaving apart the formal problem of splitting the drag in several terms, and remembering that what is to be minimized is the total drag.

A method has been widely used to examine wind-tunnel balance data, at least for engineering purpose, in which the

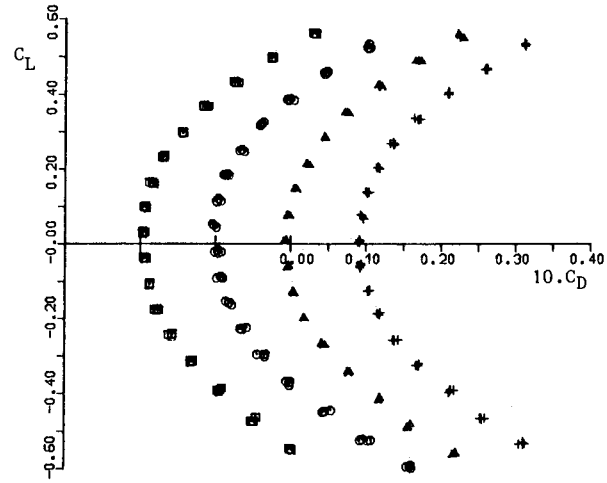

Fig. 2 Lift and drag characteristics of the four wings.

drag coefficient is supposed to be conveniently described by a parabolic form:

$$C_D(C_L) = C_{D_0} + \alpha C_L + \beta C_L^2$$

where the coefficient β includes both the pressure and friction drag dependence upon C_L^2.

Table 2 shows the coefficients obtained from a second-degree polynomial fitting, where $\sqrt{\sigma}$ is the rms value of the data fitting.

Observe that there is a global tendency for C_{D_0} to decrease with the sweep, whereas β has the opposite behavior. Introducing the efficiency $e = [\pi \cdot AR(dC_D/dC_L^2)]^{-1}$, including viscous effects, it is found that

$$e_0 = 0.92; \quad e_1 = 0.87; \quad e_2 = 0.88; \quad e_3 = 0.84$$

A better fit with the experimental data is obtained by raising the degree of the polynomial; e.g.

$$C_D(C_L) = C_{D_0} + \alpha C_L + \beta C_L^2 + \delta C_L^3 + \gamma C_L^4$$

In Table 3 the value of the zero lift drag coefficient is slightly altered in comparison with the first polynomial fitting, but the β variation is large (>10%). This suggests a nonparabolic evolution of the friction drag with lift, but we find again that β increases markedly with sweep. The corresponding efficiency factors are

$$e_0 = 1.03; \quad e_1 = 0.98; \quad e_2 = 0.96; \quad e_3 = 0.91$$

Hoerner[6] has collected data relative to the dependence of Oswald's efficiency upon the sweep angle and proposes a law in the form

$$e = \frac{1}{\cos(\phi - \phi_0)}$$

where $\phi_0 = 5$ deg.

Within the accuracy of the data, the crescent planform seems to follow this empirical rule.

The coefficient β is affected by the tunnel boundaries (image vortices model) and a rapid estimation can be obtained[5]: $\Delta C_D = 0.125(S/C) \cdot C_L^2$, where S is the wing surface (0.072 m^2), and C is the tunnel cross section (1.05 m^2). For the straight wing in infinite medium $\Delta\beta \simeq 0.009$. The streamwise position of the vortex patterns due to sweep obviously induces variations of the corrections to be applied, but this effect cannot explain the differences observed between the four wings which are of the same order.

Table 2 Parabolic regression coefficients

Model	C_{D_0}	α	β	$\sqrt{\sigma}$
0	0.00999	0.00043	0.06944	0.00060
1	0.00955	−0.00094	0.07333	0.00053
2	0.00898	0.00043	0.07238	0.00053
3	0.00898	−0.00024	0.07568	0.00050

Table 3 Polynomial coefficients (4th-deg polynomial)

Model	C_{D_0}	β	γ	$\sqrt{\sigma}$
0	0.01027	0.06157	0.02555	0.00039
1	0.00980	0.06523	0.03045	0.00039
2	0.00918	0.06664	0.01958	0.00041
3	0.00916	0.06979	0.02162	0.00042

Note: The uneven coefficients are not presented in the table for clarity.

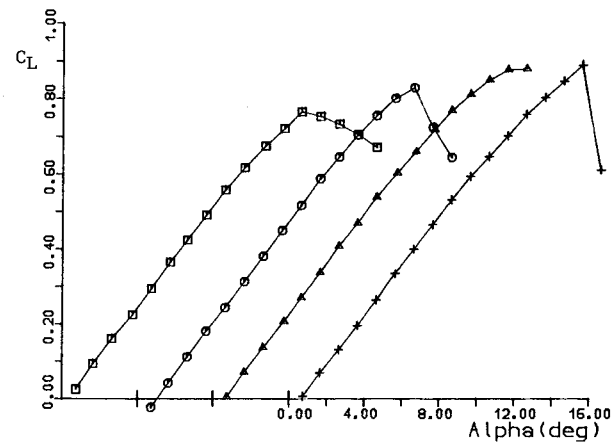

Fig. 3 Lift curves.

Note, however, that below a lift coefficient of ~0.40, the total drag is lower for the swept wing (model 4) than for the elliptical wing (model 1).

A second argument used in promoting the crescent or sheared-tip wing shapes is the behavior at stall. From Fig. 3 it is seen that a higher lift coefficient can be reached by adding sweep, at the expense of a deeper stall. The mechanism is well-known: a leading-edge conical vortex separation appears near the tips, delaying the conventional full stall.

Conclusions

The aerodynamic properties of four different wing planforms have been measured in a low-speed wind tunnel to investigate the crescent planforms, and to determine if any advantage can be drawn for aeronautical purposes. The present planforms are analytically defined with the same chord/span law (elliptical) on each model, and a variable sweep/span law varying from zero sweep to a 22.3-deg aerodynamic mean sweep. All models have a NACA 0012 section, parameters other than the sweep variation with span, are constant.

Of particular interest is the claim that the induced drag is lower over a crescent planform than on a conventional (elliptic) planform.[2-4] The classical lifting-line theory analysis of Munk[7] states that the chordwise position of the lifting elements has no effect upon the induced drag. This is obviously a first-order estimate, and from experimental compilations[5] it is commonly admitted that the sweep increases the lift-induced drag. In the present work, the total drag (pressure + friction) dependence upon the square of the lift coefficient follows the empirical rule. It is pointed out that many difficulties have to be faced to analyze the total induced drag, which moreover does not appear to be conveniently described by a parabolical relation with the lift coefficient. Therefore, the comparison has been done in terms of total drag, and the crescent planforms show a reduction of the efficiency factor as the mean sweep increases.

Despite that disappointing result, it must be noticed that below a lift coefficient of 0.40, a lower drag (10%) is observed for the crescent wing (Λ_{ma} = 22.3 deg) in comparison with the basic elliptic wing. This effect is presumed to arise from the spanwise deflection of the surface streamlines over the crescent wing, with a possible reduction of the chordwise component of the friction drag.

Another positive result is the higher maximum lift coefficient resulting from the outboard leading-edge sweep angle. Whether the two mentioned benefits of the crescent wing explain its selection by several species is an open question. Many other properties of animal lifting surfaces should be taken into account, such as flexibility, before attempting to answer the question.

This work was initiated with the hope of a possible lift-induced pressure drag reduction. From this point of view it appears that only very small (second-order) effects, positive or negative, can be expected from deviations with respect to the basic Prandtl's definition of minimum induced drag, and we can ask if the theoretical splitting between viscous and inviscid drag has to be maintained. Two reasons may be put forward. First, the assumptions required to split the drag components from wind-tunnel data involve a level of uncertainty of the same order as, or even greater than, the expected changes of the induced drag. Second, what the aeronautical engineer finally needs is a lower total drag, irrespective of the balance between the components.

References

[1]Van Dam, C. P., "Drag-Reduction Characteristics of Aft-swept Wing Tips," AIAA Paper 86-1824, June 1986.

[2]Van Dam, C. P., "Induced-Drag Characteristics of Crescent-Moon-Shaped Wings," *Journal of Aircraft*, Vol. 24, No. 2, 1987, pp. 115–119.

[3]Van Dam, C. P., Vijgen, P. M. H. W., and Holmes, B. J., "Aerodynamic Characteristics of Crescent and Elliptic Wings at High Angles of Attack," *Journal of Aircraft*, Vol. 28, No. 4, 1991, pp. 253–260.

[4]Van Dam, C. P., Vijgen, P. M. H. W., and Holmes, B. J., "Experimental Investigation of the Effect of Crescent Planform on Lift and Drag," *Journal of Aircraft*, Vol. 28, No. 11, 1991, pp. 713–720.

[5]Rae, W. H., Jr., and Pope, A., "Low-Speed Wind Tunnel Testing," Wiley, New York, 1984, pp. 376–402.

[6]Hoerner, S. F., "Fluid Dynamic Drag," Hoerner Fluid Dynamics, Albuquerque, NM, 1957, pp. 7, 8.

[7]Schlichting, H., and Truckenbrodt, E., "Aerodynamics of the Airplane," McGraw-Hill, New York, 1979, pp. 173–175.

Wake Curvature and Airfoil Lift

Lucien Z. Dumitrescu*
Université de Provence, Marseille, France

Introduction

RECENTLY, one witnesses renewed interest in the effects of wake curvature upon the flow around airfoils; sometimes, however, puzzling results are reported.[1] The purpose of this Note will be to discuss, in the light of some previous results,[2] the physics of the phenomena, which are frequently obscured by emphasis on numerics. An analogy with the jet-flap will be put forward in this context, which will throw more light upon the subject and allow assessing the relative importance of the effects involved.

Received Aug. 11, 1992; revision received Jan. 20, 1993; accepted for publication March 10, 1993.

*Invited Professor, Centre de Saint Jérôme, Case 321, 13397 Marseille Cedex 20; formerly Senior Scientific Counsellor, Institute of Aeronautics, Bucharest, Romania. Associate Fellow AIAA.

Effects of Boundary Layer and Wake upon the Lift Slope

This is a problem as old as aerodynamics itself: it is known that the lift slope of an airfoil, in incompressible flow, at moderate angles of attack (i.e., before separation sets in), is fairly well predicted by potential theory (without considering viscous effects), with only a small correction factor:

$$C_{L\alpha} = (1 - \eta)C_{L\alpha(\text{pot})} \tag{1}$$

where, for most airfoils, $C_{L\alpha(\text{pot})}$ is very close to 2π, and η is of the order of 0.1, depending slightly on the Reynolds number. Certainly, this loss is due to the development of the boundary layer, but the explicit mechanism is not obvious; sometimes, the effect of wake curvature is invoked. Therefore, the aim of the following will be to render things more explicit.

Currently, analysis of the real flow around an airfoil follows two approaches: 1) either a viscous-inviscid coupling of a potential (or Euler) solution to a boundary-layer computation (with possible iterations); or 2) a full frontal attack with the Navier-Stokes equations. While potentially able to furnish the ultimate answer, in our opinion this latter approach suffers two major drawbacks. On the one hand, even with modern hypercomputers, it is still not possible to refine the computational grids to the point of getting rid of artificial viscosity terms (which, in our belief, render questionable the whole endeavor); and, besides, this "pointillist" way of painting the reality often renders hazy the qualitative behavior of the flow and hinders attempts at reasoned modifications of the airfoil shape, to produce certain desired performance features. Subsequently, both approaches always furnish values of $C_{L\alpha}$ quite close to experiment,[3] but do not provide an explanation of the facts. One point which has frequently been raised in this connection is the influence of the wake curvature[1,4]; before discussing this question some basic theorems will be recalled.

Wake-Curvature Singularity in Potential Flow

On a lift-carrying airfoil, the streamline emerging from the trailing edge always exhibits a certain curvature, $1/\bar{r}_s$. In Ref. 2, a formula has been deduced for this quantity, depending on the flow potential $F(z)$, and on the complex function $z = f(\zeta)$, which maps the airfoil contour onto the unit circle. It has been further proved that, at the trailing edge itself, the streamline curvature is infinite (in potential flow) unless the airfoil is at a certain, singular, angle of attack α^*, whose value is proper to each particular airfoil. Furthermore, and adopting Lighthill's approach, if one considers the equivalent blunt airfoil contour, obtained by adding the boundary-layer displacement thickness to the basic section (Fig. 1) one can, in principle, write down its conformal mapping function (for a discussion of the conformal mapping of blunt—or open—contours, see Ref. 2); then the same formulas apply, and one finds the curvature along the trailing-edge streamlines. Now, based on physical reasoning, Proposition IX of Ref. 2 states that, at each angle of attack α, the interplay between the

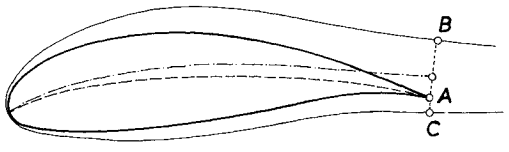

Fig. 1 Equivalent airfoil contour, generated by adding the boundary-layer thickness to the original shape.